Multistep Approach to Microscopic Models for Frustrated Quantum Magnets: The Case of the Natural Mineral Azurite

Harald Jeschke,[1] Ingo Opahle,[1] Hem Kandpal,[2] Roser Valentí,[1] Hena Das,[3] Tanusri Saha-Dasgupta,[3] Oleg Janson,[4] Helge Rosner,[4] Andreas Brühl,[5] Bernd Wolf,[5] Michael Lang,[5] Johannes Richter,[6] Shijie Hu,[7] Xiaoqun Wang,[7] Robert Peters,[8] Thomas Pruschke,[9] and Andreas Honecker[9]

[1]*Institut für Theoretische Physik, Goethe-Universität Frankfurt am Main, 60438 Frankfurt am Main, Germany*
[2]*IFW Dresden, Post Office Box 270116, 01171 Dresden, Germany*
[3]*Satyandranath Bose National Centre for Basic Sciences, Kolkata 700098, India*
[4]*Max Planck Institute for Chemical Physics of Solids, 01187 Dresden, Germany*
[5]*Physikalisches Institut, Goethe-Universität Frankfurt am Main, 60438 Frankfurt am Main, Germany*
[6]*Institut für Theoretische Physik, Universität Magdeburg, Post Office Box 4120, 39016 Magdeburg, Germany*
[7]*Department of Physics, Renmin University of China, Beijing 100872, China*
[8]*Department of Physics, Graduate School of Science, Kyoto University, Kyoto 606-8502, Japan*
[9]*Institut für Theoretische Physik, Georg-August-Universität Göttingen, 37077 Göttingen, Germany*

(Received 6 December 2010; published 23 May 2011)

The natural mineral azurite $Cu_3(CO_3)_2(OH)_2$ is a frustrated magnet displaying unusual and controversially discussed magnetic behavior. Motivated by the lack of a unified description for this system, we perform a theoretical study based on density functional theory as well as state-of-the-art numerical many-body calculations. We propose an effective generalized spin-1/2 diamond chain model which provides a consistent description of experiments: low-temperature magnetization, inelastic neutron scattering, nuclear magnetic resonance measurements, magnetic susceptibility as well as new specific heat measurements. With this study we demonstrate that the balanced combination of first principles with powerful many-body methods successfully describes the behavior of this frustrated material.

DOI: 10.1103/PhysRevLett.106.217201 PACS numbers: 75.50.Ee, 71.15.Mb, 75.10.Jm, 75.30.Et

The natural mineral azurite $Cu_3(CO_3)_2(OH)_2$ has been used as a blue pigment since the time of the ancient Egyptians; the beautiful intense blue color [see Fig. 1(a)] is due to the crystal field splitting of Cu $3d$ orbitals in square planar coordination. More recently, the discovery of a plateau at 1/3 of the saturation value in the low-temperature magnetization curve [1,2] has triggered intensive interest in the magnetic properties of azurite. From the point of view of magnetism, the most important structural motives [3] are diamondlike chains which are formed by the spin-1/2 copper atoms [Fig. 1(b)]. If all exchange constants were antiferromagnetic, azurite would fall into the class of geometrically frustrated magnets. These systems are fascinating since the competition of the magnetic interactions suppresses classically ordered states and may give rise to new states of matter with exotic excitations (see Ref. [4] for a recent review). In particular, for a certain class of frustrated magnets including diamond chains, one expects localized (dispersionless) many-body states at high magnetic fields [5]; indeed inelastic neutron scattering (INS) on azurite exhibits an almost dispersionless branch of excitations [6].

There have been a number of attempts [1,6–10] to derive a microscopic model for the complex magnetic properties of azurite. The results are, however, contradictory and up to now none of these models was able to yield a fully consistent picture of the experimentally observed behavior. Some authors favor a diamond chain model with all exchanges antiferromagnetic [1,9,11] while other authors proposed one of the dominant exchange constants to be ferromagnetic [6–8]. Even more, Ref. [10] has argued that interchain coupling is important in azurite. The latter may be in agreement with the observation of a magnetic ordering transition at about 2 K [1,12,13], but raises the question why no dispersion perpendicular to the chain direction is observed by INS [6].

In the present work, we combine first principles density functional theory (DFT) calculations with model computations based on different variants of the density-matrix renormalization group (DMRG) method [14–17] and resolve the underlying model for azurite. We find that an effective generalized spin-1/2 diamond chain model with a dominant next-nearest-neighbor antiferromagnetic Cu dimer coupling J_2, two antiferromagnetic nearest- and third-nearest-neighbor Cu dimer-monomer exchanges J_1 and J_3, and a significant direct Cu monomer-monomer exchange J_m [see Figs. 1(b) and 3(a)] explains a broad range of experiments on azurite [1,2,6,18] and resolves the existing controversies.

Since the experimentally determined positions of the lighter atoms in a structure usually carry larger error bars than those of more heavy elements, we first performed a Car-Parrinello molecular dynamics calculation [19] in order to optimize the positions of the C, O, and H atoms in azurite. With the optimized structure with a total of 30 atoms in the unit cell we determined the electronic

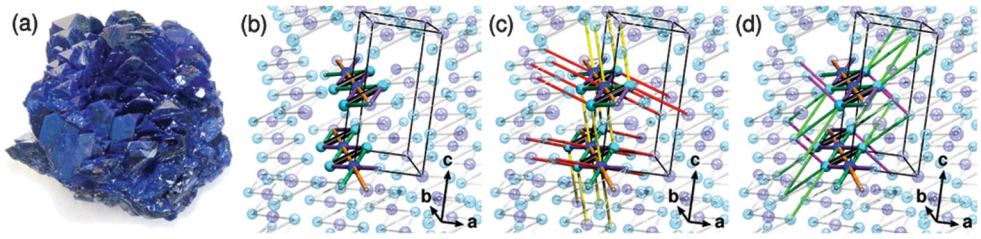

FIG. 1 (color). (a) Example of an azurite crystal aggregate. (b)–(d) Arrangement of Cu^{2+} ions in the structure of azurite. The two inequivalent Cu^{2+} ions form dimers (cyan) and monomers (blue). (b) Most important exchange paths within the diamond chain running along the b axis: Dimer coupling J_2 (black), dimer-monomer couplings J_1 and J_3 (magenta and green), and monomer-monomer coupling J_m (orange). (c)–(d) Three-dimensional couplings between diamond chains, connecting (c) monomer and dimer ions: J_5 (yellow) and J_6 (red) and (d) dimer ions only: J_4 (pink) and J_7 (light green).

properties of azurite [20]. The band structure shows six narrow Cu $3d_{x^2-y^2}$ bands at the Fermi level—corresponding to the six Cu atoms per unit cell—separated by an energy of 0.9 eV from the occupied Cu $3d_{z^2}$ bands and by a gap of $E_g \simeq 3$ eV from the higher unoccupied bands [Figs. 2(a) and 2(b)]. Figure 2(c) shows a charge density isosurface, where a $d_{x^2-y^2}$ symmetry of the Cu d orbitals is evident without contribution of d_{z^2} character, contrary to previous suggestions [21,22].

While the GGA calculation describes this system as metallic, the insulating behavior is correctly given within the GGA + U approach (see below). Here we first analyze the interaction paths based on the GGA band structure. We perform Nth order muffin tin orbital (NMTO) downfolding [23,24] to obtain the tight-binding Hamiltonian parameters t_i describing the six Cu $3d_{x^2-y^2}$ bands [see Fig. 2(b)]. Under the assumption that the exchange couplings are antiferromagnetic, we can estimate the magnitude of the exchange couplings via second-order perturbation theory: $J_i^{\mathrm{AFM}} = 4t_i^2/U$ where U is the Cu $3d$ on-site Coulomb

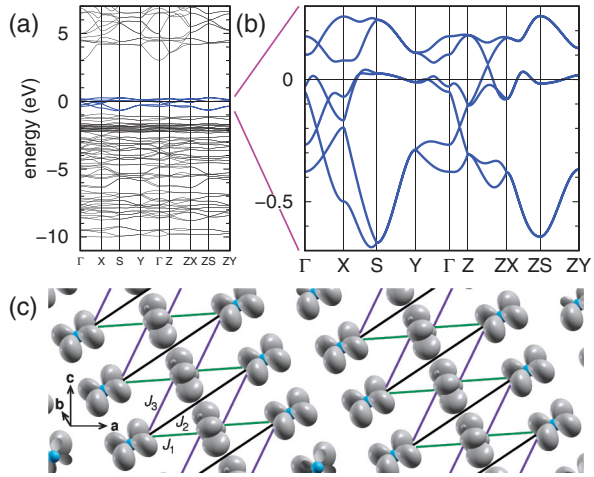

FIG. 2 (color). Electronic structure of azurite, calculated with FPLAPW. (a) Band structure in a wide energy window. At the Fermi level the bands are dominantly of Cu $3d_{x^2-y^2}$ character (blue bands). (b) Blow-up of the six bands at the Fermi level. (c) Electron density above $E = -0.75$ eV for an isovalue of 0.1 e/a.u.^{3}. All density is centered at the Cu sites and it has $3d_{x^2-y^2}$ symmetry.

interaction strength. From this analysis we identify six further relevant couplings in addition to J_1, J_2 and J_3: the monomer-monomer exchange J_m also considered by Rule *et al.* [6] and the nearest-neighbor Cu dimer interaction J_d along the chain. In addition, J_4 and J_7 provide couplings between Cu dimer atoms in neighboring chains, whereas J_5 and J_6 correspond to Cu monomer-dimer interchain interactions. The interaction paths between chains are visualized in Figs. 1(c) and 1(d).

Next, we obtain the correct sign (ferro- or antiferromagnetic) and magnitude of the J_i from total energy calculations for different Cu spin configurations in supercells with up to 60 atoms. We employ the full potential local orbital (FPLO) method [25] with the GGA + U functional for $U = 4$, 6, and 8 eV. We map the energy differences of the frozen collinear spin configurations onto a spin-1/2 Heisenberg model and evaluate the exchange constants J in a dimer approximation [26]. The nine relevant Cu-Cu interaction paths obtained from the downfolding calculations have been probed with 10 different antiferromagnetic spin configurations together with the ferromagnetic configuration. The result for a choice of $U = 8$ eV and $J_H = 1$ eV is shown in the first line of Table I. As expected from experimental observations, J_2 dominates and exhibits a $1/U$ dependence [17]. The two couplings J_1 and J_3 are very similar in magnitude, suggesting an almost symmetric diamond chain. We observe that except for J_1, J_2, and J_3, the coupling strengths are of the order of a few Kelvin. Comparing our set of parameters in Table I, line 1 to that obtained in Ref. [10], the main differences are that we determined the additional 3D couplings J_4, J_5, and J_7, and our value for J_m, double-checked with two full potential methods [20,25], is clearly nonzero.

At first sight, the fact that interchain coupling turns out to be appreciable is surprising because INS did not observe any dispersion perpendicular to the chain direction [6]. However, since the dimer exchange J_2 dominates, one can use perturbative arguments along the lines of Ref. [27] to show that there are no low-energy excitations dispersing perpendicular to the chains. The essential ingredients of the argument are that (i) the interchain exchange constants J_4 to J_7 are small compared to J_2 and (ii) they connect only to dimers of the neighboring chains [compare

TABLE I. Exchange constants in Kelvin (K) derived from FPLO GGA + U calculations with $U = 8$ eV and $J_H = 1$ eV for the various model steps considered in the present work (see text for explanation). The error margin for each J_i in the third line is estimated to be of the order 1 to 2 K.

	J_1	J_2	J_3	J_4	J_5	J_6	J_7	J_m	J_d
1 full model	13.5	42.8	12.5	2.7	0.6	4.4	−1.7	2.6	−0.4
2 minimal model	17.9	43.9	12.0	⋯	⋯	⋯	⋯	2.4	⋯
3 refined model	15.51	33	6.93	⋯	⋯	⋯	⋯	4.62	⋯
4 Ref. [1] model	19	24	8.6	⋯	⋯	⋯	⋯	⋯	⋯

Figs. 1(c) and 1(d)], i.e., they contribute only in second or third order in perturbation theory [17]; this would suggest using an effective one-dimensional model with the values of J_1, J_2, J_3, and J_m adjusted to incorporate the effect of the three-dimensional couplings. Table I line 2 shows the results obtained by solving the 10 spin configurations only for the diamond chain couplings. This corresponds to an averaging over the 3D couplings and translates into a significant asymmetry of the diamond chain $J_1 > J_3$. The effective one-dimensional model has the additional advantage that it is amenable to detailed quantum mechanical model calculations, thus allowing a quantitative comparison with experimental data for azurite.

From these results salient experimental features of azurite can already be understood at a qualitative level: two thirds of the Cu^{2+} spins are strongly bound by J_2 into dimer singlets while another third consists of monomer spins which interact weakly by J_m and additional effective monomer-monomer interactions which are generated by integrating out the dimers. In an applied magnetic field, the monomer spins are therefore polarized first while the dimer spins remain in the singlet state, giving rise to the 1/3 plateau [1,2,18]. Furthermore, the two energy scales, i.e., the low-energy scale given by the monomer-monomer interactions and the high-energy scale associated to the dimers give rise to the double-peak structures observed in the magnetic susceptibility [1] and the specific heat [1,6]. Finally, we expect a band of low-energy monomer excitations dispersing along the chain direction and a band of dimer excitations at higher energies whose dispersion is additionally suppressed by the competition of J_1 and J_3, as indeed observed by INS [6].

We will now show that we can also describe these experimental results quantitatively. The DFT results leave some freedom concerning the overall energy scale, however the ratios of the J_i are expected to be subject only to small errors [28]. We therefore first slightly refined the parameter ratios using the magnetization and INS experiments, leading to $J_1/J_2 = 0.47$, $J_3/J_2 = 0.21$, and $J_m/J_2 = 0.14$. The global energy scale is finally adjusted to the magnetization curve (see below) and we obtain the exchange coupling constants J_i in Table I, line 3.

In order to fully account for the quantum nature of the spins residing on the Cu^{2+} ions, we use a spin 1/2 Heisenberg model $\mathcal{H} = \sum_{\langle i,j \rangle} J_{i,j} \vec{S}_i \cdot \vec{S}_j - g\mu_B H \sum_i S_i^z$, where $\vec{S}_i$ are spin 1/2 operators, $J_{i,j}$ is the exchange constant connecting sites i and j [see Fig. 3(a)], H an external magnetic field and μ_B the Bohr magneton. The gyromagnetic ratio g is set to 2.06 [29].

Figure 3(b) shows a comparison for the experimental and computed magnetization curves. The overall energy scale is $J_2 = 33$ K, leading to our final parameter set in Table I, line 3. The agreement of the theoretical magnetization curve in Fig. 3(b) with the experimental result for $H \perp b$ [2] is excellent. Note that the experimental curve for $H \perp b$ exhibits a nice plateau as expected for a Heisenberg model whereas for $H \parallel b$ the plateau is washed out [1], indicative of noncommuting fields. Therefore we compare our results for the isotropic Heisenberg model with experiments for $H \perp b$. We find that dimer spins should be about 2.7% polarized each [17], i.e., dimers are essentially in the singlet state whereas the single

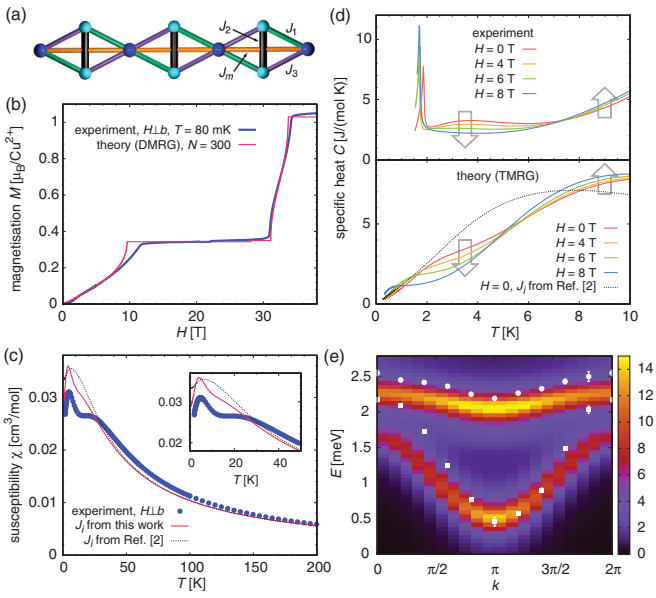

FIG. 3 (color). (a) Generalized diamond chain model. (b) Comparison of computations for the magnetization curve for $T = 0$ and $N = 300$ spins with experimental data at $T = 80$ mK for $H \perp b$ [2]. (c) Experimental and theoretical zero-field magnetic susceptibility. (d) Experimental (upper panel) and theoretical (lower panel) specific heat results for various H fields. Arrows indicate the response to increasing magnetic field. (e) Theoretical transverse dynamic structure factor on the 1/3 plateau ($H \approx 14$ T) and peak positions of INS spectra from Ref. [6] (white symbols). Color coding represents the intensity in arbitrary units.

''monomer'' spins are almost fully polarized in the 1/3 plateau. This is qualitatively consistent with recent ^{63,65}Cu NMR [18].

At this stage, the values of all J_i are fixed and we have a parameter-free prediction of the magnetic susceptibility χ. Figure 3(c) compares our computations [15] with our measurement of the magnetic susceptibility of azurite for $H \perp b$, which is very similar to the original experiment of Ref. [1]. Our parameter set (Table I, line 3) leads to a small, but qualitative improvement compared to the original one of [1] (see Table I, line 4): we reproduce a double-peak-like structure at the correct temperatures whereas only a single peak [7] is obtained with the parameters of [1].

Analogous to the magnetic susceptibility, we also have a parameter-free prediction for the magnetic specific heat. At zero-field, two anomalies have been observed in the specific heat at $T = 18$ K [1] and $T = 4$ K [1,6]. Figure 3(d) compares the field-dependence of the experimental specific heat with results calculated [15] for the parameters of Table I, line 3. The sharp peak in the experimental curves slightly below 2 K [1,12] signals an ordering transition which is out of reach of a one-dimensional model. Nevertheless, not only are the numerical values of the specific heat for $2\ \mathrm{K} < T \lesssim 10$ K comparable between theory and experiment, but also important features are reproduced correctly: (i) a low-temperature peak appears for $H = 0$ at $T \approx 3$ to 4 K. Note that this low-temperature peak at $H = 0$ is absent [8] for the original parameter set of Ref. [1] [compare the black dashed curve in the lower panel of Fig. 3(d)]. (ii) The low-temperature peak is gradually suppressed by an applied field, as emphasized by down arrows in the figure. (iii) In the temperature range $7\ \mathrm{K} \leq T \leq 10$ K, the specific heat increases not only with temperature but also with increasing magnetic field (marked by up arrows).

Figure 3(e) shows our numerical result [16,17] for the transverse dynamic structure factor on the 1/3 plateau as a function of momentum transfer k along the chain direction and energy E. The peak values of the dynamic structure factor trace two dispersion curves nicely. Comparison with the corresponding INS results [6] [white symbols in Fig. 3(e)] shows that the computed ratio of the bandwidths is extremely close to the experimental value of about 1/6 [30]. Also the total intensities in the peaks compare favorably with the experimental results [6,17].

To summarize, we have shown that the combination of first principles DFT with state-of-the-art many-body calculations successfully provides a microscopic model for the frustrated magnet azurite, which explains a wide range of experiments [1,2,6,18]. We believe that attempts to fit such a range of experiments, using at least four exchange constants J_i, are bound to fail. Hence, the guiding DFT computations were essential. There are several issues for further experimental and theoretical study [17]. In particular, the implications of the full three-dimensional model which we have derived remain to be explored.

We would like to thank H. Kikuchi and S. Süllow for providing us with the experimental data shown in Figs. 3(b) and 3(e), respectively. Useful discussions with C. Berthier, M. Horvatić, and S. Süllow are gratefully acknowledged. This work has been supported by the DFG (SFB/TR 49, SFB 602, HO 2325/4-2, PR 298/10, and RI 615/16-1), by the Helmholtz Association through HA216/EMMI, the National Natural Science Foundation of China (NSFC), and the JSPS together with the Humboldt Foundation for R. P.

[1] H. Kikuchi *et al.*, Phys. Rev. Lett. **94**, 227201 (2005).
[2] H. Kikuchi *et al.*, Prog. Theor. Phys. Suppl. **159**, 1 (2005).
[3] F. Zigan and H. D. Schuster, Z. Kristallogr. **135**, 416 (1972).
[4] C. Lacroix, P. Mendels, and F. Mila, *Introduction to Frustrated Magnetism*, Springer Series in Solid-State Sciences (Springer, Heidelberg, 2011), Vol. 164.
[5] O. Derzhko *et al.*, Low Temp. Phys. **33**, 745 (2007).
[6] K. C. Rule *et al.*, Phys. Rev. Lett. **100**, 117202 (2008).
[7] B. Gu and G. Su, Phys. Rev. Lett. **97**, 089701 (2006).
[8] B. Gu and G. Su, Phys. Rev. B **75**, 174437 (2007).
[9] H.-J. Mikeska and C. Luckmann, Phys. Rev. B **77**, 054405 (2008).
[10] J. Kang *et al.*, J. Phys. Condens. Matter **21**, 392201 (2009).
[11] H. Kikuchi *et al.*, Phys. Rev. Lett. **97**, 089702 (2006).
[12] H. Forstat *et al.*, J. Chem. Phys. **31**, 929 (1959).
[13] M. C. R. Gibson *et al.*, Phys. Rev. B **81**, 140406(R) (2010); K. C. Rule *et al.*, Phys. Rev. B **83** 104401 (2011).
[14] S. R. White, Phys. Rev. Lett. **69**, 2863 (1992).
[15] X. Wang and T. Xiang, Phys. Rev. B **56**, 5061 (1997).
[16] E. Jeckelmann, Phys. Rev. B **66**, 045114 (2002).
[17] See supplemental material at http://link.aps.org/supplemental/10.1103/PhysRevLett.106.217201.
[18] F. Aimo *et al.*, Phys. Rev. Lett. **102**, 127205 (2009).
[19] R. Car and M. Parrinello, Phys. Rev. Lett. **55**, 2471 (1985); P. E. Blöchl, Phys. Rev. B **50**, 17953 (1994).
[20] P. Blaha *et al.*, *WIEN2k: An Augmented Plane Wave Plus Local Orbitals Program for Calculating Crystal Properties.* (TU Wien, Austria, 2001).
[21] E. L. Belokoneva, Yu. K. Gubina, and J. B. Forsyth, Phys. Chem. Miner. **28**, 498 (2001).
[22] The orbital assignment is given in the local reference frame of Cu where the xy plane corresponds to the CuO_4 plane with x parallel to a Cu-O bond.
[23] O. K. Andersen and T. Saha-Dasgupta, Phys. Rev. B **62**, R16219 (2000).
[24] R. Valentí, T. Saha-Dasgupta, and C. Gros, Phys. Rev. B **66**, 054426 (2002).
[25] K. Koepernik and H. Eschrig, Phys. Rev. B **59**, 1743 (1999); http://www.FPLO.de.
[26] T. Chanier *et al.*, Phys. Rev. B **73**, 134418 (2006).
[27] A. Honecker and A. Läuchli, Phys. Rev. B **63**, 174407 (2001).
[28] H. C. Kandpal *et al.*, Phys. Rev. Lett. **103**, 067004 (2009).
[29] H. Ohta *et al.*, J. Phys. Soc. Jpn. **72**, 2464 (2003).

[30] We would like to emphasize that we have made no further adjustments to the magnetic field $H = 14$ T although the critical field at the lower edge of the $M = 1/3$ plateau is reproduced less accurately than other features [compare Fig. 3(b)]. Therefore, we attach more importance to the bandwidth ratio than the absolute position of the excitation bands.